Highly excited Σ^- states of molecular hydrogen

F. Argoubi,[1] S. Bezzaouia,[1] H. Oueslati,[1] M. Telmini,[1,2] and Ch. Jungen[3,*]

[1]*LSAMA Department of Physics, Faculty of Science of Tunis, University of Tunis El Manar, 2092 Tunis, Tunisia*

[2]*National Centre for Nuclear Science and Technology, Sidi Thabet Technopark 2020 Tunisia*

[3]*Laboratoire Aimé Cotton du CNRS, Université de Paris-Sud, F-91405 Orsay, France*

(Received 16 February 2011; published 10 May 2011)

We report calculations of H_2 Σ^- states using a variational R-matrix approach combined with multichannel quantum defect theory. Several Rydberg series converging to the $2p\pi$ state of the H_2^+ ion core are established and their mutual channel interactions characterized. The influence of the external electron on the chemical bond is found to be particularly strong in these electronically and chemically weakly bound states.

DOI: 10.1103/PhysRevA.83.052504 PACS number(s): 31.50.Df, 31.15.A−, 34.80.−i, 03.65.Nk

I. INTRODUCTION

Diatomic hydrogen is known to possess states that are highly excited electronically, yet are quite long-lived or even metastable. A familiar example is afforded by the $3p\pi\ c\,^3\Pi_u^-$ triplet levels of H_2 which are situated 13 eV above the ground state and are metastable with lifetimes ranging from 0.1 to 0.5 ms [1]. Still higher, 16 eV above the ground state—and higher than the ionization energy of H_2—singlet levels of $^1\Pi_u^-$ symmetry have been found recently to have lifetimes as long as $\approx$0.01 μs, allowing molecular fluorescence to occur despite the fact that these levels are pre-dissociated as well as autoionized [2]. In the present paper we discuss states of Σ^- electronic symmetry which are electronically stable and are situated at yet far higher energies, as much as 26 eV above the ground state.

Diatomic hydrogen is the simplest molecular system possessing more than one electron, and thus, according to the building-up principles for diatomic molecules [3], it is the smallest molecule that can have Σ^- electronic states. However, to the best of our knowledge, these states have eluded experimental observation so far. Their existence has been confirmed and some of their characteristics have been determined by theoretical calculations, initially by Martin [4] and later by Komasa [5].

Komasa [5] carried out accurate quantum chemical calculations of the lowest state for each Σ^- symmetry ($^1\Sigma_g^-$, $^3\Sigma_g^-$, $^1\Sigma_u^-$, $^3\Sigma_u^-$). He found that all these states have a minimum and may support bound rotation-vibration levels. Martin used the B-spline method [6] and calculated several higher states for each of the Σ^- manifold of symmetries [4]. His calculations however were restricted to small values of the internuclear distance R, and therefore Martin could not ascertain whether these states would have a potential minimum or not.

In this work we present calculations based on the halfium R-matrix code [7], which extend these earlier results (i) toward larger R values than considered by Martin and (ii) to higher energies as well. We show that a whole family of Σ^- states exists in the H_2 molecule, which exhibit potential minima and which form Rydberg series converging towards the H_2^+ $2p\pi$ core state. These turn out to be non-autoionizing despite their high energy. The H_2^+ $2p\pi$ state of the ion possesses a potential minimum near 8 bohrs [8] and is known to support 11 vibrational levels [9]. Preliminary R-matrix results on doubly excited states of H_2 of $^1\Sigma_g^-$ symmetry have been presented in a previous publication [10].

II. THEORY

A. General considerations

In recent years we have developed an *ab initio* R-matrix approach [7] which enables bound states and core-excited scattering states of H_2 to be calculated for fixed nuclei. Our work is based on the pioneering ideas of Greene and Yoo [11,12], which it adapts such as to yield quantum defect matrices that evolve smoothly throughout the bound and continuous energy regions, and which also vary reasonably mildly as functions of the molecular geometry (internuclear distance R). Our "halfium model" combines the variational eigenchannel R-matrix method [13] with the generalized multichannel quantum defect theory (GMQDT) [14] implemented using prolate spheroidal electron coordinates. The approach has been used to investigate singlet ungerade symmetries ($^1\Sigma_u$, $^1\Pi_u$) [7,15] and gerade symmetries ($^1\Sigma_g$, $^1\Pi_g$, $^1\Delta_g$) [16], both for the bound and the continuum (autoionization) regions.

It is interesting to note that even the most recent quantum chemical calculations [17] on H_2, while following individual potential energy curves out to large internuclear distances, are still limited to the lowest excited states since they do not exceed $n \approx 5$ (where n is the principal quantum number). The R-matrix method in general is not particularly adapted *a priori* to treat systems for very large internuclear distances, and up to date most applications have dealt with small molecules at or near their equilibrium geometries [18]. However, owing to the use of spheroidal coordinates the halfium model appears well adapted to be applied for moderately large R values. Its implementation in terms of these coordinates allows the partial wave expansion of the electron wave functions to be kept to a minimum. One of the advantages of the "halfium model" is also that it produces quantum defects which can be used directly for the calculation of the nuclear-electronic dynamics in the framework of multichannel quantum defect theory (MQDT). The halfium scheme together with the MQDT framework leads to a global analysis of the interactions as no distinction is made between "open" and "closed" channels

*Also at: Department of Physics and Astronomy, University College London, London WC1E 6BT, United Kingdom.

at the outset, but instead all channels are treated on the same footing irrespective of their corresponding channel thresholds. In this picture doubly excited states are included explicitly as electron-ion collision channels in their own right. It has further been shown how MQDT can describe competing ionization and dissociation processes [19], and include rovibrational dynamics via the frame transformation technique [20]. Therefore MQDT possesses all the ingredients to address the problem competing dissociation and ionization processes affecting quasibound states (resonances), and, when combined with the halfium model, it is capable to yield *ab initio* predictions of such processes as well.

The previous implementations of the molecular variational R-matrix method [7,11,12] made no distinction between channels of Σ^+ and Σ^- symmetry. In other words, the symmetry property of the electron wave function obtained by a reflection of all electron coordinates at a plane containing the two nuclei (symmetry operation σ_v) was not introduced explicitly. We reformulate the halfium approach here such as to include this symmetry property. We have shown previously [10] how the convergence in the calculation of $^1\Sigma_g^+$ states is improved by this extension.

In the original formulation of the halfium model [7,12] each calculation was performed separately for each molecular symmetry defined by the standard quantum numbers Λ (projection of the angular momentum on the internuclear axis, taken positive), electron spin ($S = 0,1$), and *gerade* or *ungerade* [$(-1)^p$ with $p = 0$ or 1]. From elementary molecular theory [21] we know that in a diatomic molecule the symmetry operation σ_v corresponding to a reflection of all electron coordinates at any plane containing the two nuclei also commutes with the electronic Hamiltonian so that an additional quantum number arises: the electronic wave function has negative symmetry ($q = 1$) or positive symmetry ($q = 0$) depending on whether it changes sign or not upon reflection. Σ symmetry ($\Lambda = 0$) is the only symmetry for which the q quantum number is relevant at the electronic stage of calculation [22,23]. As far as molecular hydrogen is concerned, the σ_v symmetry may in practice be disregarded even for Σ states as long as energies below $2p\sigma$ ion threshold are considered. The reason is that only Σ^+ states arise in this range. Indeed, the lowest Σ^- state occurs associated with the $(2p\pi)\epsilon p\pi$ configuration and is expected to lie at around 27 eV above the ground state. The Σ^- states are thus well separated from Σ^+ states, and for many practical purposes they need not be taken into consideration.

B. Symmetrized R-matrix code for $\Lambda = 0$ states

In what follows we describe the main modifications required in the halfium model in order to take account of the σ_v symmetry for $\Lambda = 0$ states. The code may be used to calculate $\Lambda \neq 0$ states as previously [7]. In the halfium model, the two-electron configuration space is divided into two regions: (i) a reaction volume where the variational R-matrix method is employed, and (ii) the remaining space, called asymptotic zone, where GMQDT is used. The connection of the inner zone and outer zone wave functions yields the desired reaction matrix or the equivalent quantum defect matrix.

Each two-electron basis function defined in the reaction zone is expressed in spheroidal coordinates (ξ,η,φ) and corresponds to a configuration i,j (cf. [7,12]) with a specified set of quantum numbers $\{S,\Lambda,p,q\}$:

$$\overline{y}_{ij}(\vec{r_1},\vec{r_2}) = \overline{N}_{ij}[y_{ij}^{+-}(\vec{r_1},\vec{r_2}) + (-1)^q y_{ij}^{-+}(\vec{r_1},\vec{r_2})]. \quad (1)$$

$\vec{r_1}$ and $\vec{r_2}$ are the position vectors of each electron defining the corresponding spheroidal coordinates (ξ,η,φ). The functions y_{ij}^{+-} and y_{ij}^{-+} are products of one-electron orbitals characterized by *signed* orbital angular momentum components:

$$y_{ij}^{+-}(\vec{r_1},\vec{r_2}) = N_{ij}[\phi_i^+(\vec{r_1})\phi_j^-(\vec{r_2}) + (-1)^S\phi_j^-(\vec{r_1})\phi_i^+(\vec{r_2})], \quad (2)$$

$$y_{ij}^{-+}(\vec{r_1},\vec{r_2}) = N_{ij}[\phi_i^-(\vec{r_1})\phi_j^+(\vec{r_2}) + (-1)^S\phi_j^+(\vec{r_1})\phi_i^-(\vec{r_2})].$$

Here

$$\begin{aligned}\phi_i^{\pm}(\vec{r}) &= \frac{\chi_i(\xi)}{\sqrt{\xi^2-1}}\frac{\zeta_i(\eta)}{\sqrt{1-\eta^2}}\frac{1}{\sqrt{2\pi}}\exp(\pm i\lambda_i\varphi) \\ &\equiv \frac{\chi_i(\xi)}{\sqrt{\xi^2-1}}Y_{\ell_i,\pm\lambda_i}(\eta,\varphi) \quad (3)\end{aligned}$$

is the ith one-electron wave function of H_2^+. We shall below designate each one-electron function defined by Eq. (3) by the short-hand ket notation $|i^{\pm}\rangle = |n_i\ell_i\lambda_i^{\pm}\rangle$, where it is understood that in the ket notation $\lambda_i^+ = |\lambda_i|$ and $\lambda_i^- = -|\lambda_i|$. The total symmetry Λ of a two-electron function according to Eq. (2) thus corresponds to $|\lambda_i^+ + \lambda_j^-| = 0$. It is further implied here and later in this section that ℓ_i is the generalized orbital angular momentum quantum number arising when spheroidal coordinates are used [7]. The factors $Y_{\ell\lambda}(\eta,\varphi)$ on the second line of Eq. (3) thus are normalized spheroidal harmonics, analogous to the familiar spherical harmonics. The one-electron functions $|i^{\pm}\rangle$ are therefore *gerade* when ℓ is even, and they are *ungerade* when ℓ odd. The desired symmetry g/u of the two-electron functions is thus $(-1)^p = (-1)^{\ell_i+\ell_j}$, and is obtained by appropriately combining even and/or odd ℓ orbitals. For this reason the quantum number p does not appear explicitly in Eqs. (1) and (2). The normalization factors N_{ij} and $\overline{N}_{ij}$ are given in the Appendix. The basis of two-electron functions $\overline{y}_{ij}$ used in the variational R-matrix approach consists both of "closed" functions whose radial component $\chi^{(c)}(\xi_0)$ vanishes on the reaction surface ξ_0, and of "open" functions whose radial component $\chi^{(o)}(\xi_0)$ is nonzero but has a vanishing radial derivative on the reaction surface ξ_0 [7,11].

The two-electron basis functions are used to solve the Schrödinger equation inside the reaction volume in the framework of the variational R-matrix method. The procedure outlined in Ref. [7] remains the same, but, because of the symmetrization, each matrix element taken in the basis of the two-electron wave functions $\overline{y}_{ij}$ now becomes a sum over four terms. This is detailed in the Appendix. The eigensolutions are denoted $\overline{\Psi}_\beta(\vec{r_1},\vec{r_2})$, where β is a solution index, and are characterized by stationary logarithmic derivatives b_β on the reaction surface $\max(\xi_1,\xi_2) = \xi_0$. They are obtained inside the reaction volume as an expansion over the two-electron configurations,

$$\overline{\Psi}_\beta = \sum_{ij} c_{ij}^\beta \overline{y}_{ij}, \quad (4)$$

which is the σ_v-symmetrized version of Eq. (10) of Ref. [7].

Each solution $\overline{\Psi}_\beta$ may be continued in the external zone, i.e., for radii of the outer electron larger than ξ_0, as a linear combination of regular and irregular two-center Coulomb radial functions,

$$\overline{\Psi}_\beta(E,\omega,\xi \geqslant \xi_0) = \sum_k \overline{\Phi}_k(E,\omega)\frac{1}{\sqrt{\xi^2-1}} \times [f_k(\epsilon_c,\xi)I_{k\beta}(E) - g_k(\epsilon_c,\xi)J_{k\beta}(E)]. \tag{5}$$

Here E is the total energy, $\epsilon_c = E - E_c$ is the energy of the outer electron (with E_c the energy of the residual core), and ω stands for all coordinates except the radial coordinate of the outermost electron. The summation index k runs over those channels $k \equiv i'j'$ which are taken into account explicitly in the asymptotic zone. The matching of the outer and inner eigensolutions defines the coefficient matrix elements $I_{k\beta}$ and $J_{k\beta}$ that appear on the right-hand side of Eq. (5). This equation also shows how the matching involves expanding each inner-zone variational solution Ψ_β on the reaction surface in terms of so-called "surface harmonics" $\overline{\Phi}_k(\omega)$, for each asymptotic channel k (see [7]) and for each solution β. The form of these surface harmonics as well as their symmetrization and normalization is detailed in the Appendix.

By projecting each R-matrix eigensolution $\overline{\Psi}_\beta(\overrightarrow{r_1},\overrightarrow{r_2})$ onto a surface harmonic $\overline{\Phi}_k(\omega)$ at $\xi = \xi_0$, one obtains surface expansion coefficients $\overline{u}_{k\beta}(\xi_0)$ of the form

$$\overline{u}_{k\beta}(\xi_0) = \langle\langle \overline{\Phi}_k(\omega)|\overline{\Psi}_\beta(\omega,\xi_0)\rangle\rangle = f_k(\xi_0)I_{k\beta} - g_k(\xi_0)J_{k\beta} \tag{6}$$

(where the energy dependences have been omitted for clarity). The detailed expression of the projection integral $\langle\langle \ldots \rangle\rangle$ (integration over ω) is given in the Appendix. In order to ensure the continuity of the wave function as well as of its derivative across the reaction surface, the projection integrals $\overline{u}_{k\beta}$ must also satisfy the following equation:

$$b_\beta \overline{u}_{k\beta}(\xi_0) = f'_k(\xi_0)I_{k\beta} - g'_k(\xi_0)J_{k\beta}, \tag{7}$$

where b_β is the logarithmic derivative for each variational solution β obtained in constructing the expansion Eq. (4), and the primes refer to the radial derivative.

By combining the matching conditions, Eqs. (6) and (7), we determine the matrices $\mathbf{I}$ and $\mathbf{J}$ and hence the short-range reaction matrix $\mathbf{K} = \mathbf{J}\mathbf{I}^{-1}$ and equivalent quantum defect matrix.

C. Bound states

The spheroidal quantum defect matrix may be produced in two equivalent forms, both defined in terms of the $\mathbf{K}$ matrix [20]:

$$\boldsymbol{\mu} = \frac{1}{\pi}\arctan[\mathbf{K}], \qquad \overline{\boldsymbol{\mu}} = \mathbf{U}\left\{\frac{1}{\pi}\arctan[\mathbf{U}^{\mathbf{T}}\mathbf{K}\mathbf{U}]\right\}\mathbf{U}^{\mathbf{T}}, \tag{8}$$

where $\mathbf{U}$ is the eigenvector matrix of $\mathbf{K}$. Although both forms have strictly the same physical content, it has been found in previous applications that the matrices $\overline{\boldsymbol{\mu}}$ often exhibit a smoother dependence as function of the energy, and therefore we have used them in the present work as well. The spheroidal (two-center) quantum defect matrices may finally be converted into equivalent spherical (single-center) matrices $\overline{\boldsymbol{\mu}}$ using the techniques described in Refs. [16] and [24]. We have used both the spheroidal and the spherical forms of the quantum defect matrices.

Bound electronic states are obtained by standard MQDT procedures as previously [7] through application of the appropriate MQDT bound state boundary condition

$$\det|\tan\boldsymbol{\beta}(E) + \mathbf{K}(E,R)| = 0. \tag{9}$$

In order to solve Eq. (9), we need the reaction matrix $\mathbf{K}$ for arbitrary E. We evaluate it for each R by inverting the second Eq. (8), using the interpolated matrices $\overline{\boldsymbol{\mu}}(E)$. $\beta_i(E)$ is the accumulated radial phase in each channel i at the energy E. If the spherical formulation is used, $\beta_i(E) = \pi\nu_i$ where ν_i is equal to the usual effective principal quantum number n^* for $n^* \geqslant \ell + 1$, but differs from it for lower n^* values [24]. If spheroidal quantum defects are used, Eq. (9) remains formally unchanged, but the accumulated phase parameter $\beta_i(E)$ must now be evaluated numerically for every energy E, by solving the Schrödinger equation for radial motion of the Rydberg electron in spheroidal coordinates, and hence extracting the phase by using the techniques of generalized quantum defect theory [14]. We have ascertained that both methods yield identical effective principal quantum numbers to within < 0.002.

III. RESULTS

A. Numerical details

The reaction boundary is preferably chosen as small as possible, but must be large enough so that the $2p\pi$ core orbital is enclosed within the reaction zone. The present calculations have been carried out by using reaction boundaries corresponding to $\xi_0 = 20/R + 1$ (where R is in a.u.), chosen such that the energy of the confined core orbital deviates from the exact value of the free ion by less than about 10^{-4} a.u. The internuclear separation R has been taken to vary from 1 to 10 or 12 bohrs. The CI expansion Eq. (4) in the reaction zone included typically 200 configurations $\overline{y}_{ij}$ of the type $\pi\pi'$ and $\delta\delta'$ with ℓ,ℓ' ranging from 1–4, and with two open functions per $\ell\lambda$ value of the more highly excited electron. The following channels k were included in the asymptotic expansion Eq. (5) of the wave function:

$$^1\Sigma_g^-, {}^3\Sigma_g^- \ : (2p\pi)\epsilon p\pi \ , \ (2p\pi)\epsilon f\pi,$$
$$^1\Sigma_u^-, {}^3\Sigma_u^- \ : (2p\pi)\epsilon d\pi \ , \ (2p\pi)\epsilon g\pi.$$

The reaction matrix $\mathbf{K}$ and the equivalent quantum defect matrix $\overline{\boldsymbol{\mu}}$ were evaluated, typically, for about 100 energies on a grid chosen relative to the H_2^+ $2p\pi$ threshold which ranged from about -0.13 a.u. up to $+0.10$ a.u. The calculation of bound state energies was then carried out by suitably interpolating $\mathbf{K}$ for arbitrary energies E. We have verified that our own code reproduces the H_2^+ ion $2p\pi$ energies given by Madsen and Peek [25] to within 10^{-6} a.u.

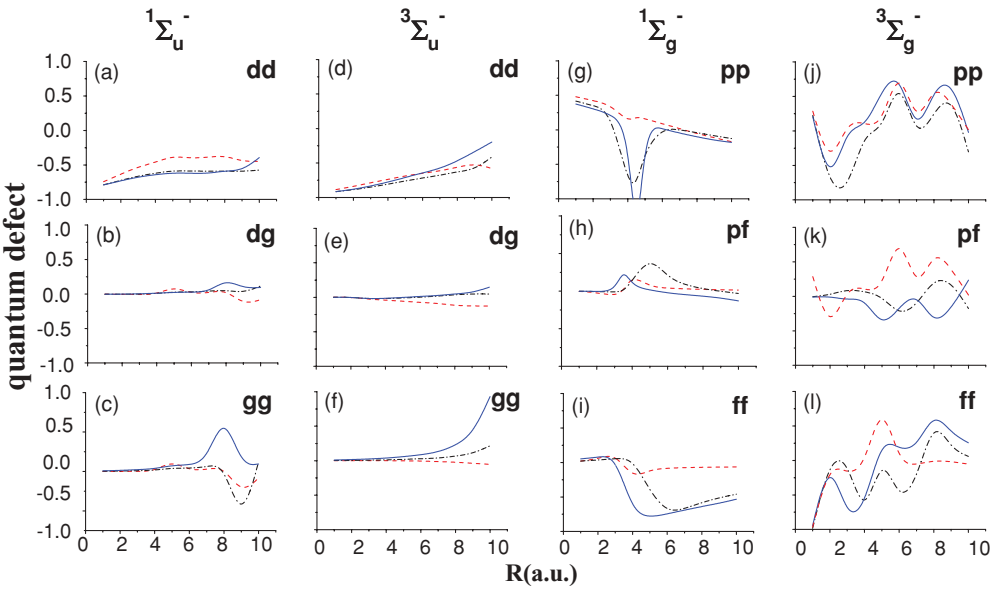

FIG. 1. (Color online) Quantum defect matrix elements $\overline{\mu}_{\ell,\ell'}$ for core excited Σ^- states of H_2 plotted as functions of the internuclear distance R. The orbital angular momentum quantum numbers $\ell\ell'$ are indicated in each panel as dd, pp, etc. Different curves in each panel correspond to different electron energies ϵ: Dashed lines (red online): bound region. Dashed-dotted lines (black): near threshold energy. Solid line (blue online) continuum region. The energies (in Rydbergs) are: Bound $^1\Sigma_u^-$ −0.16, $^3\Sigma_u^-$ −0.15,$^1\Sigma_g^-$ −0.18, $^3\Sigma_g^-$ −0.24. Threshold $^1\Sigma_u^-$ −0.02, $^3\Sigma_u^-$ −0.03,$^1\Sigma_g^-$ −0.07, $^3\Sigma_g^-$ −0.08. Continuum $^1\Sigma_u^-$ +0.02, $^3\Sigma_u^-$ +0.02,$^1\Sigma_g^-$ +0.04, $^3\Sigma_g^-$ +0.06.

B. Quantum defects

Figure 1 displays the matrix elements of the 2×2 Σ^- quantum defect matrices obtained in the present work. Each matrix element is plotted individually as a function of the internuclear distance R, with different curves representing the values obtained for different energies as indicated. The energies are in Rydbergs and are taken relative to the $2p\pi$ core state, so that negative values refer to the bound state region whereas positive values refer to the ionization continuum. As stated in Sec. III A, the singlet and triplet *ungerade* Σ^- states correspond to channels $(2p\pi)\epsilon d\pi$ and $(2p\pi)\epsilon g\pi$, respectively, whereas the singlet and triplet *gerade* Σ^- states correspond to channels $(2p\pi)\epsilon p\pi$ and $(2p\pi)\epsilon f\pi$, respectively. With the exception of $p\pi$, all the outer electrons are characterized by relatively high-ℓ orbital momenta, so that at least for small R they are nonpenetrating and are anticipated to have rather small quantum defect values. The data plotted in Fig. 1 indeed verify this expectation: for small R only the pp matrix elements differ appreciably from zero (*modulo* 1), and it may also be seen that the nondiagonal ℓ-mixing matrix elements are all small as well. These off-diagonal elements all increase substantially as R increases, reflecting the increasing departure of the molecule from spherical symmetry.

The evolution with R of the diagonal quantum defect matrix elements reflects their bonding or antibonding characteristics. The one-channel R-dependent Rydberg equation

$$U_n(R) = U^+(R) - \frac{1}{[n-\mu(R)]^2} \tag{10}$$

(written here in Rydberg units) represents the molecular Rydberg potential energy curve as a sum of the ion core potential $U^+(R)$ ($H_2^+ 2p\pi$ in the present case) and a term due to the Rydberg electron. As recognized by Mulliken [26], the R-dependent Rydberg equation shows how a quantum defect curve that has a *positive* slope as function of R will *weaken* the molecular bond because the effective principal quantum number $n^* = n - \mu$ *decreases* with R. Conversely, a quantum defect that has a *negative* slope will tend to *strengthen* the bond. Inspection of Fig. 1 indicates that the $p\pi$ Rydberg electron is bonding, whereas the $d\pi$ and $f\pi$ electrons are antibonding, and the high-ℓ $g\pi$ electron is essentially nonbonding. This

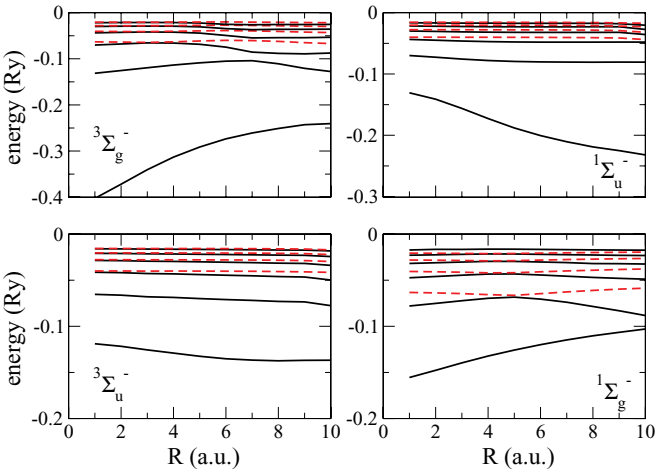

FIG. 2. (Color online) Rydberg binding energies for core excited Σ^- states of H_2 plotted as functions of the internuclear distance R. The states corresponding for small R to lower orbital angular momentum are represented by full (black) lines. Those corresponding to higher orbital angular momentum are represented by dashed (red online) lines.

TABLE I. Clamped-nuclei effective principal quantum numbers n^* for Σ^- Rydberg series in H_2. R is the internuclear distance in a.u., Δn^* are differences with respect to the values obtained by Martin [4].

$R =$	1		2		3		4		5		6	7	8	9	10
	n^*	Δn^*	n^*	Δn^*	n^*	Δn^*	n^*	Δn^*	n^*	Δn^*	n^*	n^*	n^*	n^*	n^*
$^3\Sigma_g^- 2p\pi$	1.576	−0.007	1.640	−0.007	1.714	−0.006	1.787	−0.005	1.853	−0.005	1.912	1.958	1.996	2.029	2.039
$3p\pi$	2.759	−0.004	2.823	−0.000	2.894	0.004	2.968	0.011	3.032	0.015	3.085	3.100	3.004	2.879	2.799
$4p\pi$	3.776	−0.004	3.838	−0.006	3.906	0.017	3.897	0.067	3.819	0.088	3.659	3.419	3.367	3.347	3.381
$4f\pi$	3.976	0.029	3.961	0.040	3.937	0.030	3.975	0.002	4.036	0.002	4.083	4.067	4.009	3.921	3.862
$5p\pi$	4.781	−0.020	4.842	−0.034	4.885	−0.011	4.864	0.039	4.754	0.052	4.497	4.277	4.294	4.296	4.333
$5f\pi$	4.967		4.948		4.938		4.977		5.037		5.081	5.035	4.961	4.871	4.816
$6p\pi$	5.784		5.844		5.856		5.849		5.715		5.377	5.207	5.262	5.264	5.294
$6f\pi$	5.963		5.943		5.961		5.978		6.038		6.080	6.007	5.931	5.847	5.796
$7p\pi$	6.785		6.846		6.868		6.841		6.688		6.292	6.179	6.247	6.244	6.275
$7f\pi$	6.961		6.941		6.950		6.978		7.038		7.080	6.987	6.914	6.835	6.787
mean value		−0.001		−0.001		0.007		0.023		0.031					
$^1\Sigma_g^- 3p\pi$	2.536	0.002	2.602	0.005	2.676	0.006	2.750	0.010	2.820	0.012	2.888	2.952	3.011	3.064	3.117
$4p\pi$	3.580	0.008	3.647	0.007	3.720	0.006	3.789	0.003	3.824	0.045	3.766	3.679	3.569	3.468	3.365
$4f\pi$	3.976	0.029	3.959	0.038	3.936	0.047	3.903	0.061	3.880	0.024	3.934	3.992	4.045	4.092	4.129
$5p\pi$	4.594	0.000	4.661	0.002	4.735	−0.004	4.804	−0.009	4.811	0.024	4.749	4.680	4.613	4.564	4.524
$5f\pi$	4.966	0.014	4.946	0.011	4.917	0.021	4.878	0.031	4.883	−0.018	4.945	5.004	5.048	5.104	5.141
$6p\pi$	5.600		5.668		5.742		5.812		5.806		5.747	5.685	5.589	5.581	5.549
$6f\pi$	5.962		5.941		5.910		5.870		5.888		5.951	6.011	6.066	6.110	6.147
$7p\pi$	6.604		6.672		6.746		6.816		6.805		6.746	6.687	6.641	6.589	6.558
$7f\pi$	6.960		6.938		6.906		6.866		6.891		6.955	7.014	7.067	7.114	7.150
$8p\pi$	7.606		7.764		7.746		7.822		7.804		7.746	7.689	7.633	7.593	7.563
mean value		0.011		0.013		0.015		0.019		0.017					
$^3\Sigma_u^- 3d\pi$	2.900	0.001	2.867	0.000	2.822	−0.005	2.784	−0.003	2.747	−0.003	2.720	2.705	2.698	2.703	2.704
$4d\pi$	3.912	0.001	3.886	0.007	3.834	−0.003	3.816	0.024	3.781	0.045	3.753	3.729	3.701	3.687	3.589
$5d\pi$	4.915	−0.013	4.888	−0.011	4.835	−0.015	4.813	0.011	4.770	0.037	4.733	4.700	4.658	4.633	4.480
$5g\pi$	4.999	0.023	4.998	0.027	4.990	0.034	4.993	0.052	4.989	0.065	4.983	4.979	4.959	4.939	4.905
$6d\pi$	5.916	−0.336	5.889	−0.330	5.834	−0.377	5.808	−0.375	5.762	−0.342	5.720	5.683	5.633	5.605	5.431
$6g\pi$	5.998		5.996		5.987		5.989		5.981		5.972	5.963	5.932	5.895	5.794
$7d\pi$	6.917		6.890		6.833		6.805		6.756		6.711	6.672	6.619	6.589	6.405
$7g\pi$	6.997		6.995		6.985		6.986		6.976		6.964	6.953	6.914	6.867	6.701
$8d\pi$	7.916		7.887		7.846		7.794		7.744		7.705	7.665	7.607	7.577	7.390
$8g\pi$	7.996		7.994		7.984		7.984		7.973		7.959	7.945	7.903	7.847	7.636
mean value		−0.065		−0.062		−0.073		−0.058		−0.040					
$^1\Sigma_u^- 3d\pi$	2.766	−0.001	2.662	−0.002	2.530	−0.004	2.406	−0.001	2.306	0.000	2.233	2.179	2.137	2.108	2.076
$4d\pi$	3.782	0.007	3.709	0.014	3.634	0.024	3.580	0.035	3.545	0.045	3.529	3.523	3.519	3.522	3.521
$5d\pi$	4.786	−0.004	4.717	0.006	4.649	0.013	4.602	0.017	4.573	0.020	4.562	4.561	4.561	4.566	4.565
$5g\pi$	4.999	0.023	4.998	0.027	4.996	0.040	4.993	0.052	4.988	0.064	4.982	4.972	4.955	4.925	4.772
$6d\pi$	5.787	−0.465	5.720	−0.359	5.655	−0.287	5.611	−0.245	5.586	−0.242	5.577	5.578	5.580	5.585	5.589
$6g\pi$	5.998		5.996		5.993		5.988		5.980		5.970	5.954	5.923	5.850	6.052
$7d\pi$	6.788		6.723		6.659		6.616		6.592		6.585	6.588	6.589	6.592	6.599
$7g\pi$	6.997		6.995		6.991		6.985		6.975		6.962	6.942	6.901	6.763	6.999
$8d\pi$	7.788		7.722		7.664		7.656		7.596		7.590	7.593	7.595	7.459	7.611
$8g\pi$	7.996		7.994		7.989		7.983		7.972		7.957	7.932	7.885	7.760	
mean value		−0.088		−0.063		−0.043		−0.028		−0.022					

behavior is in line with the general expectations of bonding characteristics of molecular orbitals established in the early times of quantum mechanics [3,27,28]. This point will be discussed further in Secs. III C and III E below.

Figure 1 shows that superimposed on these general trends the H_2 Σ^- symmetry quantum defects exhibit strong combined energy and coordinate dependences in certain ranges. For instance, the $^1\Sigma_g^-$ quantum defects (third column of panels from the left) exhibit quite strong such dependences, which peak near the $2p\pi$ threshold for $R \approx 5$. The ℓ-mixing matrix element pf is seen to exhibit a strong peak in this range. However, this is not necessarily just ℓ mixing

due to the increasing nonsphericity of the molecule, but it may well be related also to configuration mixing involving doubly excited channels deriving from higher thresholds as for instance from the $3d\pi$ threshold. Such channels are not included explicitly in the asymptotic zone expansion Eq. (5) (summation over k) in our R-matrix treatment. However, since the inner-zone expansion Eq. (4) includes such configurations, interactions of this type may cause R-matrix poles to occur which yield energy dependences in the quantum defects.

C. Rydberg binding energies and effective principal quantum numbers

Solution of Eq. (9) yields sets of Rydberg binding energies $\epsilon_n(R)$ corresponding to the second term of Eq. (10). These are displayed in Fig. 2. Each panel of Fig. 2 contains two interacting R-dependent Rydberg series. The series which corresponds to the lower ℓ component for small R are represented by full (black online) curves in each panel, whereas the corresponding higher ℓ components are drawn as dotted (red online) lines. The bonding character of the $p\pi$ series and the antibonding character of the $d\pi$ series are clearly visible for the *gerade* $^{1,3}\Sigma_g^-$ and *ungerade* $^{1,3}\Sigma_u^-$ symmetries, respectively (full curves with positive and negative slopes in the various panels).

An interesting aspect of the $^{1,3}\Sigma_g^-$ are the avoided crossings, due to ℓ-mixing interaction (ℓ,ℓ' off-diagonal quantum defect matrix elements), that occur between the states corresponding to the bonding $np\pi$ and the antibonding $nf\pi$ Rydberg electrons. These appear clearly for the $^1\Sigma_g^-$ symmetry near $R \approx 5$ a.u., and are even more pronounced near $R \approx 7$ a.u. for the $^3\Sigma_g^-$ symmetry. We shall discuss this aspect further in Sec. III D below.

Table I lists for each symmetry the effective principal quantum numbers $n^*(R) = n - \mu(R)$, evaluated with Eq. (10), of the first ten electronic states obtained in this work. The differences with respect to the results of Martin are also included whenever the corresponding data are available in Ref. [4]. The present effective quantum numbers are seen to agree with the data derived from Ref. [4] to within about 0.01 for the lowest states and to within 0.03 for higher states. Exceptions occur for each of the *ungerade* symmetries, where the highest state calculated by Martin differs substantially from ours, by as much as 0.2 to 0.4. As demonstrated by Table I and Fig. 3, our calculations predict rather regular Rydberg series throughout the ranges of energy and internuclear distance considered here, and therefore we suspect that the highest states calculated in Ref. [4] might be less accurate. On the other hand, it is apparent from Table I that the present calculations provide a more comprehensive picture of the way the Σ^- Rydberg series evolve with internuclear distance and energy.

The effective principal quantum numbers for all four symmetries are also represented graphically in Fig. 3 as functions of R. Notice how for small R the lowest $^3\Sigma_g^-$ state corresponds to $n^* \approx 1.6$ (penetrating $2p\pi$ electron, π^2 configuration) whereas the $^1\Sigma_g^-$ series starts out with $n^* \approx 2.5$ ($3p\pi$ electron, $\pi\pi'$ configuration)—in line of course with the standard building up principles for diatomic molecules [3].

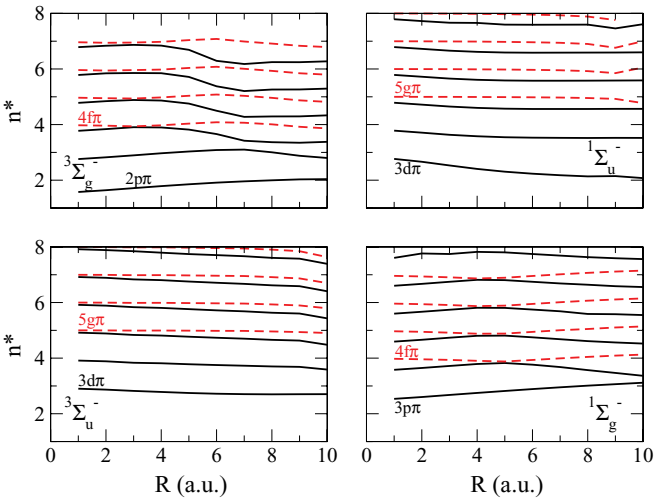

FIG. 3. (Color online) Effective principal quantum numbers for core excited Σ^- states of H_2 plotted as functions of the internuclear distance R. The states corresponding for small R to lower orbital angular momentum are represented by full (black) lines. Those corresponding to higher orbital angular momentum ar represented by dashed (red online) lines. The quantum numbers of the outer electron are indicated for the lowest series member of each series.

The $^{1,3}\Sigma_u^-$ $d\pi$ series start out at the $n^* \approx 2.8$ level as expected for weakly penetrating $3d\pi$ electrons. The avoided crossings which occur in the *gerade* manifolds are well borne out in this plot.

D. Potential energy curves

Potential energy curves are calculated from the Rydberg binding energies according to Eq. (10) by addition of the H_2^+ ion $2p\pi$ potential energy curve $U^+(R)$. Tables II and III contain the numerical values thus obtained for the lowest Σ^- state for each of the four symmetries. For the purpose of comparison the corresponding values from Martin [4] and Komasa [5] are also included in the tables. Assuming that the potential energy curves obtained in Ref. [5] are quasiexact, we see that our results are, in the average, about 150 cm^{-1} too high. In terms of quantum defects this means that the effective principal quantum numbers produced by our R-matrix and MQDT code are by about 0.01 too large. Inspection of Tables II and III further shows that—with the exception of the lowest $^1\Sigma_g^-$ state—our electronic energies are systematically *lower* than those of Martin [4], which indicates that they are somewhat better converged. Figure 4 is a graphical representation of the lowest Σ^- potential energy curves which highlights the reasonable agreement between the present calculations and those of Komasa [5]. We expect that the higher potential energy curves calculated with the R-matrix method for each symmetry are progressively more accurate as the energy increases. This has been demonstrated previously in the case of the $^1\Sigma_g^+$ states of H_2 [16].

Since the H_2^+ $2p\pi$ core has a rather shallow potential energy curve with a correspondingly large equilibrium distance, 7.93 a.u., the effect of the outer molecular electron on the bond length is comparatively strong, making the Σ^- Rydberg series a textbook example for studying the bonding characteristics

TABLE II. Electronic energies of the lowest $^3\Sigma^-$ states of H_2. Internuclear distance R and energies E are in atomic units, energy differences ΔE are in cm^{-1}. E_H present work. E_M is from Martin [4]. E_K is Komasa [5]. $\Delta E_{HM/K} = 2\mathcal{R}(E_H - E_{M/K})$, where $\mathcal{R}$ is the Rydberg constant. Note that in order to obtain total energies one has to add the nuclear repulsion term $1/R$ to the energies E.

	$^3\Sigma_g^-$					$^3\Sigma_u^-$				
R	E_H	E_M	E_K	ΔE_{HM}	ΔE_{HK}	E_H	E_M	E_K	ΔE_{HM}	ΔE_{HK}
1.0	−0.675 53	−0.6737	−0.676 21	−401	151	−0.533 55	−0.5336	−0.534 04	12	110
1.5	−0.645 67	−0.6439	−0.646 10	−388	94	−0.511 79	−0.5118	−0.512 30	3	112
2.0	−0.614 67	−0.6130	−0.614 89	−365	50	−0.489 62	−0.4896	−0.490 12	−4	109
2.5	−0.584 59	−0.5832	−0.584 83	−305	52	−0.468 47	−0.4685	−0.469 04	7	125
3.0	−0.556 63	−0.5554	−0.556 79	−269	37	−0.449 25	−0.4490	−0.449 61	−54	81
3.5	−0.530 89	−0.5298	−0.531 07	−240	38	−0.431 65	−0.4313	−0.431 94	−77	65
4.0	−0.507 42	−0.5066	−0.507 63	−179	49	−0.415 32	−0.4152	−0.415 95	−25	139
5.0	−0.466 95	−0.4662	−0.467 12	−165	38	−0.387 65	−0.3875	−0.388 31	−33	146
6.0	−0.433 74		−0.433 95		46	−0.364 56		−0.365 36		176
7.0	−0.406 54		−0.406 91		80	−0.344 94		−0.345 97		226
8.0	−0.385 00		−0.385 05		12	−0.328 22		−0.329 31		240
9.0	−0.366 45		−0.367 63		260	−0.313 48		−0.314 81		293
10.0	−0.352 95		−0.353 91		210	−0.301 09		−0.302 07		216
mean value				−289	86				−21	160

of molecular orbitals. This is illustrated by Fig. 5 which displays the $^3\Sigma_g^-$ and $^1\Sigma_g^-$ potential energy curves of H_2. The bonding and antibonding effects are clearly visible and are quite substantial for low n^*. The two interleaved series show nicely the opposite effects of the bonding $p\pi$ and antibonding $f\pi$ orbitals: the former is seen to shorten the equilibrium separation substantially, whereas the latter lengthens it, to the extent that for instance the second $^1\Sigma_g^-$ potential curve is purely repulsive beyond $R = 10$ bohrs. For higher n^* the R_e values progressively approach the ion value. On the other hand, for the *ungerade* symmetries the nonbonding character of the $d\pi$ orbital alters the R_e value only little with respect to that of the ion core.

E. Dissociation behavior of the π^2 and $\pi\pi'$ Σ^- Rydberg states

We complete this section by briefly considering the dissociation behavior of the Σ^- H_2 Rydberg states. Martin [4] has previously discussed this point, but as in our opinion his conclusions are partly incorrect, we repeat the discussion here. Σ^- states can arise in a two-electron system only from π^2, δ^2, . . .and $\pi\pi'$, $\delta\delta'$, . . . configurations. The states calculated

TABLE III. Electronic energies of the lowest $^1\Sigma^-$ states of H_2. Internuclear distance R and energies E are in atomic units, energy differences ΔE are in cm^{-1}. E_H present work. E_M is from Martin [4]. E_K is Komasa [5]. $\Delta E_{HM/K} = 2\mathcal{R}(E_H - E_{M/K})$, where $\mathcal{R}$ is the Rydberg constant. Note that in order to obtain total energies one has to add the nuclear repulsion term $1/R$ to the energies E.

	$^1\Sigma_g^-$					$^1\Sigma_u^-$				
R	E_H	E_M	E_K	ΔE_{HM}	ΔE_{HK}	E_H	E_M	E_K	ΔE_{HM}	ΔE_{HK}
1.0	−0.551 85	−0.5520	−0.552 29	32	97	−0.539 46	−0.5394	−0.539 92	−13	100
1.5	−0.527 60	−0.5278	−0.528 05	45	99	−0.519 35	−0.5193	−0.519 80	−11	99
2.0	−0.502 62	−0.5029	−0.503 10	61	104	−0.499 35	−0.4992	−0.499 82	−32	104
2.5	−0.478 60	−0.4789	−0.479 14	67	120	−0.480 92	−0.4808	−0.481 42	−25	112
3.0	−0.456 29	−0.4566	−0.456 83	68	119	−0.464 54	−0.4643	−0.465 03	−53	108
3.5	−0.435 72	−0.4361	−0.436 34	83	136	−0.450 01	−0.4499	−0.450 57	−23	123
4.0	−0.416 92	−0.4174	−0.417 62	105	155	−0.437 17	−0.4371	−0.437 77	−14	132
4.5	−0.399 89	−0.4004	−0.400 57	113	150	−0.425 78	−0.4257	−0.426 35	−18	126
5.0	−0.384 25	−0.3848	−0.385 02	121	169	−0.415 38	−0.4154	−0.416 07	5	152
5.5	−0.370 05		−0.370 84		175					
6.0	−0.356 92		−0.357 89		213	−0.397 29		−0.398 14		188
7.0	−0.334 02		−0.335 21		261	−0.381 91		−0.382 94		225
8.0	−0.314 67		−0.316 17		330	−0.369 04		−0.369 87		183
9.0	−0.298 28		−0.300 20		421	−0.357 50		−0.358 60		242
10.0	−0.284 19		−0.286 86		585	−0.348 68		−0.348 88		44
mean value				77	209				−20	138

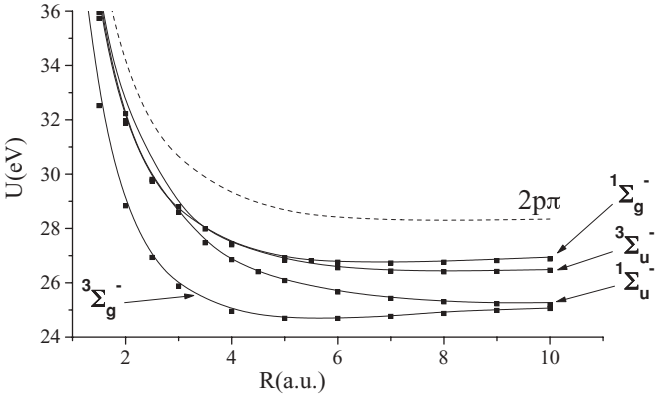

FIG. 4. The four lowest Σ^- potential energy curves of H_2. Full lines: present results. Squares: Komasa [5]. The energy, in eV, is taken with respect to the ground level of H_2. The potential energy curve of the H_2^+ $2p\pi$ core state is also shown (dashed lines).

here correspond to a $2p\pi$ ion core which correlates with the $H^+ + H(n = 2)$ dissociation limit of the ion. Therefore, starting out from the $H(n = 2)$+$H(n)$ molecular dissociation limits we need to consider only π^2 and $\pi\pi'$ configurations because $H(n = 2)$ does not support a $d\delta$ orbital. Figure 6 presents the qualitative energy correlation diagram which we obtain. The figure caption lists the detailed rules which have been applied. Unlike Martin, we find that the correlation is different for each of the four Σ^- symmetries. Specifically, the lowest $^1\Sigma_u^-$ state must correlate with the $(n = 2) + (n = 2)$ SA limit and not $(n = 2) + (n = 3)$ as indicated in Ref. [4].

Mulliken [29], in a remarkably insightful paper which has received comparatively limited attention, discussed the dissociation behavior of Rydberg states in general. He showed that in odd-electron molecules [like nitric oxide (NO) for instance] the core and the Rydberg electron follow their route to dissociation essentially independently, because configuration mixing (CM) effects which would blur the correlation rules are relatively minor ("minor CM"). By contrast in even-electron molecules like H_2 "major CM" occurs, because the SA states are in fact "entangled," that is, they are for symmetry reasons

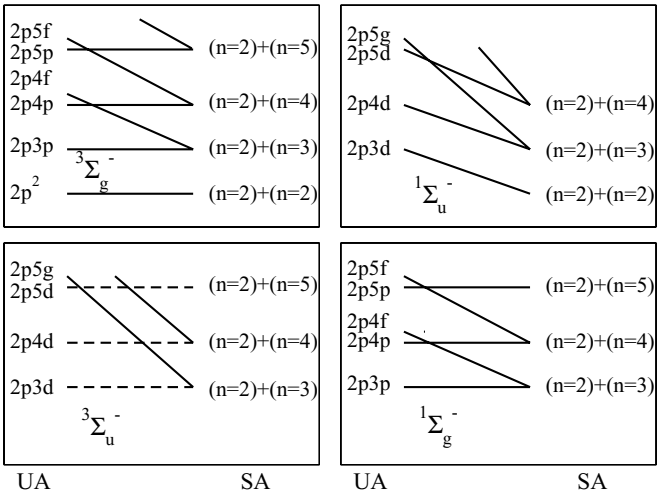

FIG. 6. Qualitative energy correlation diagram for core excited Σ^- states of H_2 between united atom (UA) and separated atom (SA) states. The states represented correspond to $(2p\pi)n\ell\pi$ configurations with $\ell \leqslant 4$. The diagram has been drawn by considering the two-electron states arising (i) in the UA and (ii) in the SA limits, based on the familiar building-up principles for symmetric diatomic molecules [3], and considering separated atom orbitals with ℓ up to 4. (iii) Further, where possible (full lines), the correlation has been made by applying the correlation rules for the one-electron H_2^+ orbitals with $\lambda = 1$ to the outer electron ($n \to n$ for $\ell = 1$, $n \to n - 1$ for $\ell = 2$ and 3, $n \to n - 2$ for $\ell = 4$ and 5). Dashed lines correspond situations where this is not possible.

strong mixtures of different electronic configurations. The dissociation behavior can therefore only formally be attributed to the Rydberg electron alone. Nevertheless, Fig. 6 shows that, neglecting ℓ mixing, in three out of the four Σ^- symmetries, the correlation remains in line with that expected for the one-electron two-center system (full lines in Fig. 6). In the fourth symmetry, $^3\Sigma_u^-$, even this formal correlation is violated (dashed lines).

Referring now to Fig. 3 we see that the behavior of the *gerade* molecular states corresponds quite nicely to that

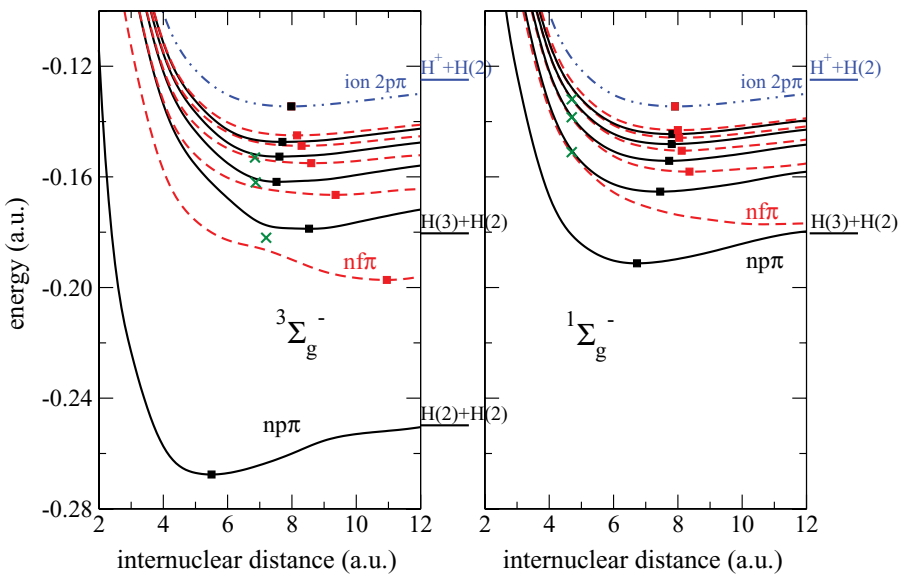

FIG. 5. (Color online) $^3\Sigma_g^-$ and $^1\Sigma_g^-$ potential energy curves of H_2 corresponding to bonding $np\pi$ and antibonding $nf\pi$ Rydberg orbitals [full lines (black) and broken lines (red online), respectively]. Filled squares indicate the positions of the potential minima. Crosses (green online) indicate the occurrence of $p \sim f$ avoided crossings. Note that owing to these avoided crossings the curves change their character in these ranges. The potential energy curve of the H_2^+ $2p\pi$ core state is also shown [dashed-dotted line (blue online)].

predicted by Fig. 6, with the additional feature that the crossings of different ℓ curves are avoided. The same can be said about the $^1\Sigma_u^-$ symmetry despite the fact that the avoided crossing do not appear clearly. However, in the $^3\Sigma_u^-$ case the avoided crossings are now so strong that the pattern of Fig. 6 is not obvious.

IV. CONCLUSION

In this work we have extended previous theoretical work [4,5] on Σ^- states in H_2, (i) by calculation of a number of higher states and (ii) by carrying the calculations to larger R values than had been done previously (except for the lowest state of each manifold). Comparison with the earlier computations, where possible, indicates that our R-matrix approach, while not approaching the state-of-the-art quantum chemical calculations of Ref. [5], is reasonably accurate and reliable, and has the advantage that arbitrarily high n values as well as continuum states can be evaluated. Further, as mentioned above, the R-matrix method is expected to yield higher potential energy curves with increasing accuracy.

We have established the existence of numerous Rydberg series which converge to the $2p\pi$ ion core threshold. Some of these series have been found to interact via ℓ-mixing interaction—an interaction which no doubt in part is induced also by configuration mixing involving yet higher ion core states. These electronic couplings lead to series of avoided crossings of the potential energy curves for some of the symmetries (cf. Figs. 2 and 3). The states involved in the crossings themselves have rather strongly varying shapes due to the bonding or antibonding effect of the Rydberg electron, respectively, which is unusually dominant here. We thus predict that the H_2 $^1\Sigma^-$ electronic states form patterns that do not conform to the traditional picture of Rydberg potential curves which converge to the ion threshold neatly stacked and nested.

Clearly these complications have to be taken into account when the nuclear dynamics is calculated. Komasa [5] predicted vibration-rotation levels for the lowest state in each of the four symmetry manifolds based on the Born-Oppenheimer approximation. We plan to calculate higher levels as well, by using multichannel quantum defect theory (MQDT) which should also account for nonadiabatic interactions such as they likely arise as a consequence of the avoided crossings.

As pointed out by the previous authors, the Σ^- states of H_2 are not affected by electronic autoionization, i.e., electronic interactions with electronic continua associated with lower H_2^+ thresholds. This fact distinguishes them from all other core excited Rydberg series, which typically are broad and in addition are mostly repulsive. Rovibronic autoionization however is possible, since for instance the Σ^- levels may be autoionized (and in fact also be pre-dissociated) through rotational ℓ-uncoupling interaction with Π^- and Δ^- continua associated with lower thresholds.

The $N = 0$ rotational levels associated with the Σ^- states are an exception here: they have *negative* total parity and therefore cannot interact with any lower levels or continua of the same N value since these have *positive* total parity without any exception. They may be affected by hyperfine or spin effects, but these are likely to be extremely weak. The only efficient way for the Σ^- $N = 0$ levels to relax energetically is by an optical electric-dipole $P(1)$ transition terminating on a lower Π^- $N = 1$ level. These transitions originate from much larger internuclear distances than the equilibrium geometries of most of the lower states on which they may terminate. They might therefore give rise to a structured emission continuum, a so-called "diffraction band," such as predicted by Condon [30] and observed previously by Dalgarno, Herzberg, and Stephens [31] in the $B - X$ transition of H_2. The theoretical study of all of these dynamical aspects is underway.

ACKNOWLEDGMENTS

Ch.J. was supported in part by the ANR (France) under Contract No. 09-BLAN-020901. F.A. and Ch.J. have also benefitted from support by the E. Miescher Foundation (Basel, Switzerland). We are grateful to Dr. A. Dora (Orsay) for helpful comments.

APPENDIX

Owing to Eq. (1), any symmetrized matrix element $\overline{A}_{ij,i'j'}$ (where $A = O, L, \frac{1}{r_{12}}, H, \Gamma$, or Λ), takes the form

$$\overline{A}_{ij,i'j'} = \overline{N}_{ij}\overline{N}_{i'j'}[(A_{i^+j^-,i'^+j'^-} + A_{i^-j^+,i'^-j'^+}) + (-1)^q(A_{i^+j^-,i'^-j'^+} + A_{i^-j^+,i'^+j'^-})]. \quad \text{(A1)}$$

[Note incidentally that the normalization factors of the present Eqs. (1), (2), and (A1), introduced originally in Ref. [7], are redefined here, with $N_{ij}(\text{previous}) = (2N_{ij}^2)^{-1}(\text{present})$]. In order to write the four terms in the above equation in a compact way, we use p or m exponents to stand for either (+) or (−) signs indifferently ($p = \pm, m = \mp$). Consequently, with Eq. (2),

$$A_{i^pj^m,i'^pj'^m} = N_{i^pj^m}N_{i'^pj'^m}[(\langle i^pj^m|A|i'^pj'^m\rangle + \langle i^mj^p|A|i'^mj'^p\rangle) + (-1)^S(\langle i^pj^m|A|i'^mj'^p\rangle + \langle i^mj^p|A|i'^pj'^m\rangle)]. \quad \text{(A2)}$$

The normalization factors $N_{i^pj^m}$ and $\overline{N}_{ij}$ thus become

$$N_{i^pj^m} = \{2[o_{i^pi^p}o_{j^mj^m} + (-1)^S|o_{i^pj^m}|^2]\}^{-\frac{1}{2}}$$
$$\overline{N}_{ij} = \{2[O_{i^pj^m,i^pj^m} + (-1)^q O_{i^pj^m,i^mj^p}]\}^{-\frac{1}{2}}. \quad \text{(A3)}$$

Here the one-electron overlap matrix element $o_{i^pj^m}$ is given by $o_{i^pj^m} = \delta(\lambda_i^p, \lambda_j^m)\hat{o}_{ij}$, with

$$\hat{o}_{ij} = \left(\frac{R}{2}\right)^3\left[\int_1^{\xi_0}\chi_i(\xi)\chi_j(\xi)d\xi\int_{-1}^{+1}\frac{\zeta_i(\eta)\zeta_j(\eta)}{1-\eta^2}d\eta + \int_1^{\xi_0}\frac{\chi_i(\xi)\chi_j(\xi)}{\xi^2-1}d\xi\int_{-1}^{+1}\zeta_i(\eta)\zeta_j(\eta)d\eta\right] \quad \text{(A4)}$$

[cf. Eq. (3) of Ref. [7]]. Note that $\delta(\lambda_i^p, \lambda_j^m) \neq 0$ if $\lambda_i^p = \lambda_j^m = 0$ (σ-type orbitals). The two-electron overlap matrix elements $O_{i^pj^m,i'^pj'^m}$ are obtained from Eq. (A2) by setting $A = 1$.

Taking account of the reflection symmetry we write the surface harmonics that appear in Eq. (5) as

$$\overline{\Phi}_k(\omega) = \overline{N}_{\Phi_k}[\Phi_k^{+-}(\omega) + (-1)^q\Phi_k^{-+}(\omega)] \quad \text{(A5)}$$

with

$$\Phi_k^{+-}(\omega) = N_{\Phi_k^{+-}}\phi_{i'}^{+}(\overrightarrow{r}_<)Y_{\ell_{j'}\lambda_{j'}^{-}}(\eta_>,\varphi_>),$$
$$\Phi_k^{-+}(\omega) = N_{\Phi_k^{-+}}\phi_{i'}^{-}(\overrightarrow{r}_<)Y_{\ell_{j'}\lambda_{j'}^{+}}(\eta_>,\varphi_>). \quad \text{(A6)}$$

The index k here stands for a particular two-electron basis function which connects to an asymptotic channel k [Eq. (5)], i.e., $k = i'j'$, with the primes used to distinguish the surface harmonic two-electron functions from those, ij, used in the expansion Eq. (4) of the solutions Ψ_β inside the reaction zone. The symbols $<$ and $>$ designate the inner and outermost electron, respectively; they originate from the indiscernibility of the electrons. $Y_{\ell\lambda}(\eta,\varphi)$ are the normalized spheroidal harmonics associated with each channel, as defined in Eq. (3). The requirement $\langle\langle\overline{\Phi}_k|\overline{\Phi}_k\rangle\rangle = 1$ yields the normalization factors N_{Φ_k} and $\overline{N}_{\Phi_k}$ as follows:

$$N_{\Phi_k^{+-}} = N_{\Phi_k^{-+}} = N_{\Phi_k} = [\hat{o}_{i',i'}]^{-\frac{1}{2}},$$
$$\overline{N}_{\Phi_k} = \{2[1+(-1)^q\delta(\lambda_{j'}^{-},\lambda_{j'}^{+})]\}^{-\frac{1}{2}}. \quad \text{(A7)}$$

If $\overline{\Phi}_k$ is associated with a Σ symmetry channel built on a σ symmetry $H_2{}^+$ ion core state, i.e., the channel corresponds to $(n\ell\sigma)\epsilon\ell'\sigma$, then $\lambda_{j'}^{-} = \lambda_{j'}^{+}$ and $\overline{N}_{\Phi_k} = 1/2$. Otherwise, $\overline{N}_{\Phi_k} = 1/\sqrt{2}$.

Finally, the surface expansion coefficient of Eq. (6) becomes

$$\overline{u}_{k\beta} = \overline{N}_{\Phi_k}\sum_{ij} c_{ij}^{\beta}\chi_j^o(\xi_0)\int_{-1}^{+1}\frac{\zeta_{\ell_{j'},\lambda_{j'}}^{\epsilon_c}(\eta)\zeta_{\ell_j,\lambda_j}(\eta)}{1-\eta^2}d\eta$$
$$\times\hat{o}_{ii'}\{[\delta(\lambda_{i'}^{+},\lambda_i^{+})\delta(\lambda_{j'}^{-},\lambda_j^{-}) + \delta(\lambda_{i'}^{-},\lambda_i^{-})\delta(\lambda_{j'}^{+},\lambda_j^{+})]$$
$$+(-1)^q[\delta(\lambda_{i'}^{-},\lambda_i^{+})\delta(\lambda_{j'}^{+},\lambda_j^{-}) + \delta(\lambda_{i'}^{+},\lambda_i^{-})\delta(\lambda_{j'}^{-},\lambda_j^{+})]\}. \quad \text{(A8)}$$

Note that, as indicated in this expression, only the "open" basis functions $\chi_j^{(o)}(\xi_0)$ contribute to the sum in Eq. (A8). Further, the expression in the last bracket [...] of Eq. (A8) is seen to vanish unless channels $(n\ell\sigma)\epsilon\ell'\sigma$ are involved.

[1] W. Lichten, Bull. Am. Phys. Soc. Ser. II **7**, 43 (1962).
[2] M. Glass-Maujean, Ch. Jungen, H. Schmoranzer, A. Knie, I. Haar, R. Hentges, W. Kielich, K. Jänkälä, and A. Ehresmann, Phys. Rev. Lett. **104**, 183002 (2010).
[3] G. Herzberg, *Spectra of Diatomic Molecules* (Krieger, Malabar, 1991).
[4] F. Martin, J. Phys. B **32**, L181 (1999).
[5] J. Komasa, Phys. Chem. Chem. Phys. **10**, 3383 (2008).
[6] F. Martin, J. Phys. B **32**, R197 (1999).
[7] M. Telmini and Ch. Jungen, Phys. Rev. A **68**, 062704 (2003).
[8] D. R. Bates, K. Ledsham, and A. L. Stewart, Philos. Trans. R. Soc. London A **246**, 215 (1953).
[9] D. M. Bishop, S. K. Shih, C. L. Beckel, F. M. Wu, and J. M. Peek, J. Chem. Phys. **26**, 145 (1975).
[10] S. Bezzaouia, F. Argoubi, M. Telmini, and Ch. Jungen, J. Phys. Conf. Ser. (in press).
[11] C. H. Greene and B. Yoo, J. Phys. Chem. **99**, 1711 (1995).
[12] B. Yoo, Ph.D. thesis, Louisiana State University, Baton Rouge, LA 1990.
[13] C. H. Greene, Phys. Rev. A **28**, 2209 (1983).
[14] Ch. Jungen and F. Texier, J. Phys. B **33**, 2495 (2000).
[15] H. Oueslati, M. Telmini, and Ch. Jungen, Mol. Phys. **104**, 187 (2006).
[16] S. Bezzaouia, M. Telmini, and Ch. Jungen, Phys. Rev. A **70**, 012713 (2004).
[17] G. Corongiu and E. Clementi, Int. J. Quant. Chem. (published online 19 AUG 2010).
[18] J. Tennyson, Phys. Rep. **491**, 29 (2010).
[19] A. Matzkin, Ch. Jungen, and S. C. Ross, Phys. Rev. A **62**, 062511 (2000).
[20] S. C. Ross and Ch. Jungen, Phys. Rev. A **49**, 4353 (1994).
[21] L. Landau and E. Lifschitz, *Quantum Mechanics* (Mir Editions, Moscow, 1966).
[22] J. Xie and R. N. Zare, J. Chem. Phys. **93**, 3033 (1990).
[23] Ch. Jungen and G. Raseev, Phys. Rev. A **57**, 2407 (1998).
[24] R. Guérout, Ch. Jungen, H. Oueslati, S. C. Ross, and M. Telmini, Phys. Rev. A **79**, 042717 (2009).
[25] M. M. Madsen and J. M. Peek, At. Data Nucl. Data Tables **2**, 171 (1971).
[26] R. S. Mulliken, J. Am. Chem. Soc. **91**, 4615 (1969).
[27] F. Hund, Z. Phys. **63**, 719 (1930).
[28] R. S. Mulliken, Rev. Mod. Phys. **4**, 1 (1932).
[29] R. S. Mulliken, J. Am. Chem. Soc. **88**, 1849 (1966).
[30] E. U. Condon, Phys. Rev. **32**, 858 (1928).
[31] A. Dalgarno, G. Herzberg, and T. L. Stephens, Astrophys. J. Lett. **162**, L49 (1970).